Resource

Cell Reports

Large-Scale Identification of Coregulated Enhancer Networks in the Adult Human Brain

Graphical Abstract

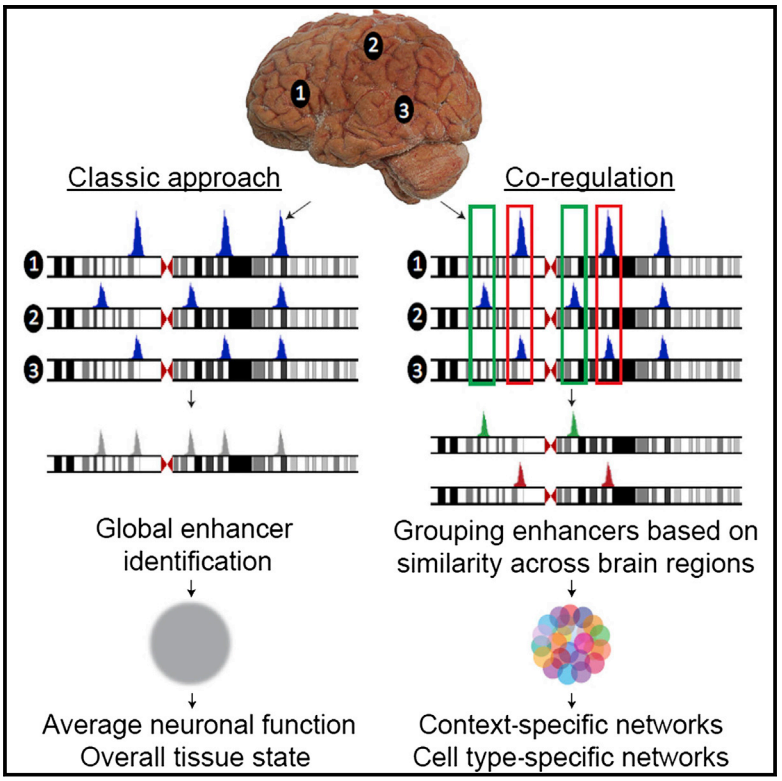

Authors

Marit W. Vermunt, Peter Reinink, ..., Edwin Cuppen, Menno P. Creyghton

Correspondence

m.creyghton@hubrecht.eu

In Brief

Epigenomic analysis of complex tissues such as the human brain has been hampered by their significant heterogeneity. However, cell culture systems and model organisms generally do not correctly represent the epigenome as it is in vivo. In this study, Vermunt et al. use large-scale ChIP-sequencing analysis to map active regulatory elements in the human brain. Analyzing activity patterns across different anatomical regions enables the identification of enhancer networks that provide cell-type and context-specific in vivo information.

Highlights

Genome-scale enhancer identification is done in 136 regions of the adult human brain

Enhancer enrichment varies across anatomical regions

Coregulated enhancers represent cell type- and context-specific networks

Alterations in newly identified enhancers are linked to Parkinson's disease risk

Vermunt et al., 2014, Cell Reports 9, 767–779
October 23, 2014 ©2014 The Authors
http://dx.doi.org/10.1016/j.celrep.2014.09.023

Cell Reports
Resource

Large-Scale Identification of Coregulated Enhancer Networks in the Adult Human Brain

Marit W. Vermunt,[1,3] Peter Reinink,[1,3] Jeroen Korving,[1] Ewart de Bruijn,[1] Paul M. Creyghton,[1] Onur Basak,[1] Geert Geeven,[1] Pim W. Toonen,[1] Nico Lansu,[1] Charles Meunier,[1] Sebastiaan van Heesch,[1] Netherlands Brain Bank,[2] Hans Clevers,[1] Wouter de Laat,[1] Edwin Cuppen,[1] and Menno P. Creyghton[1,*]
[1]Hubrecht Institute-KNAW & University Medical Center Utrecht, Uppsalalaan 8, 3584CT, Utrecht, the Netherlands
[2]Netherlands Institute for Neuroscience, Meibergdreef 47, 1105 BA, Amsterdam, the Netherlands
[3]Co-first author
*Correspondence: m.creyghton@hubrecht.eu
http://dx.doi.org/10.1016/j.celrep.2014.09.023

SUMMARY

Understanding the complexity of the human brain and its functional diversity remain a major challenge. Distinct anatomical regions are involved in an array of processes, including organismal homeostasis, cognitive functions, and susceptibility to neurological pathologies, many of which define our species. Distal enhancers have emerged as key regulatory elements that acquire histone modifications in a cell- and species-specific manner, thus enforcing specific gene expression programs. Here, we survey the epigenomic landscape of promoters and *cis*-regulatory elements in 136 regions of the adult human brain. We identify a total of 83,553 promoter-distal H3K27ac-enriched regions showing global characteristics of brain enhancers. We use coregulation of enhancer elements across many distinct regions of the brain to uncover functionally distinct networks at high resolution and link these networks to specific neuroglial functions. Furthermore, we use these data to understand the relevance of noncoding genomic variations previously linked to Parkinson's disease incidence.

INTRODUCTION

Understanding the human brain is one of the key challenges of biology. Over 100 different anatomical structures are connected by billions of neurons and glia into a functional network that regulates tissue homeostasis throughout the body while also determining our cognitive state (Nolte, 2009). Functionally distinct anatomical regions have evolved in a species-specific manner, giving rise to the defining physical and cognitive features that separate humans from other species (Konopka and Geschwind, 2010). Microarray analyses on distinct regions of the human brain have demonstrated that gene expression profiles vary significantly across adult brain structures (Colantuoni et al., 2011; Hawrylycz et al., 2012; Kang et al., 2011). The nature of these variations in gene expression and their implications in neuronal plasticity are currently subjects of intense investigation.

The epigenetic landscape that imposes these gene expression programs is regulated by transcription factors that alter local chromatin state of the genome at functional regulatory elements (e.g., enhancers and promoters). During development of the brain, progressive epigenetic alterations of the genome are involved in establishing specific functional regions (Dulac, 2010). Indeed, variations in the levels of individual transcription factors that drive these epigenetic alterations can affect functional regionalization as well as the laminar identity of cells within a given cortical region (Sur and Rubenstein, 2005). As the epigenome is influenced by environmental factors, it functions at the intersection between the genome and its developmental and environmental history. Charting the epigenome has provided crucial information on how a cell uses the epigenome to store memories of environmental events (Ostuni et al., 2013). Furthermore, it allowed the stratification of inactive gene expression states into primed/poised (ready for activation) or silent (Bernstein et al., 2006), which provides unique information on a cell's transcriptional potential.

While the core promoter of a gene constitutes the site where the transcriptional initiation complex is formed, enhancer elements are defined as regions in the genome that regulate core-promoter activity independent of distance or orientation (Maston et al., 2006). The distinction between proximal enhancers that are often coined as part of the promoter (or proximal promoter) and enhancers that are more distal is vague, but both can be considered part of the promoter as a whole. Enhancers in particular have been shown to support core promoter activity in a tissue- and species-specific manner, thus enforcing specific gene expression programs that shape the biological state of the cell (Bulger and Groudine, 2011). Enhancers can be characterized on a global scale using distinct epigenetic footprints that are typically found to display this cell type- and species-specific distribution and contain important information on how and why certain cellular states are reached (Creyghton et al., 2010; Heintzman et al., 2009; Rada-Iglesias et al., 2011; Visel et al., 2009). This information is typically missed in genome sequencing and transcriptomic studies. More recent efforts have also focused on the identification of enhancers using enhancer RNAs (eRNAs) (Andersson et al., 2014). However, this analysis

underrepresents the total amount of enhancers found by an order of magnitude (Shen et al., 2012; Zhu et al., 2013).

Others have begun to annotate distal enhancers in the mouse cortex and neural cultures (Meissner et al., 2008; Rada-Iglesias et al., 2011; Visel et al., 2013). However, most distal elements identified using these epigenetic footprints are not well conserved across species(Bernstein et al., 2012; Odom et al., 2007; Schmidt et al., 2010; Visel et al., 2013). Furthermore, the in vitro culturing of neuronal cells means replacing their physiologically relevant environment with an artificial one, which along with the unrestricted growth of cultured cells translates into multiple nonphysiological changes in the epigenetic landscape (Baylin and Ohm, 2006; Meissner et al., 2008). As such, epigenomic analysis of human tissue is currently gaining focus. Recent analyses have included the epigenetic annotation of enhancers in seven areas of the human brain and one fetal cortex (Visel et al., 2013; Zhu et al., 2013). However, as the brain harbors many functionally distinct anatomical regions, these data sets are likely an underrepresentation of the total amount of enhancers that is active in the brain.

Here we analyze the epigenome of enhancers in 136 samples covering 87 distinct anatomical regions of the adult human brain. We generate a large compendium of over 83,000 distal regulatory elements (i.e., enhancers) and use these data to analyze complex coregulated networks of enhancers in heterogeneous anatomical regions. This greatly increases the resolution of epigenomic analyses in complex tissue. Furthermore, we provide evidence for the involvement of enhancer elements in the α-synuclein and PARK16 loci as contributing factors to Parkinson's disease (PD).

RESULTS

Genome-wide Epigenomic Analysis of Active *cis*-Regulatory Elements in the Human Brain

To identify distal enhancers in different anatomical regions of the human brain, we performed ChIP-sequencing (ChIP-seq) analysis for histone 3 lysine 27 acetylation (H3K27ac) on postmortem brain tissue. This histone modification was previously shown to specifically label both active enhancers as well as active promoters (Creyghton et al., 2010; Rada-Iglesias et al., 2011; Wang et al., 2008). As the resolution of this histone mark lies within the 1–2 kb range, we defined enhancers as being enriched regions that completely fall outside of a 2 kb region around known core promoters or transcriptional start sites (TSSs), which for simplicity are just referred to as promoters. As individual variation of donors was recently demonstrated to account for significant sample to sample variation in epigenetic chromatin profiles (Kasowski et al., 2013; Kilpinen et al., 2013; McDaniell et al., 2010; McVicker et al., 2013), we performed most of our experiments using samples collected from two complete left hemispheres from two healthy female donors (hemispheres 1 and 2) (Figure S1; Table S1), as well as samples obtained from four additional donors (two male and two female). Hemispheres 1 and 2 were of comparable agonal state and differed only by their age and postmortem delay (PMD), determined as the time between death and end of abduction (Table S1). The latter is unlikely to affect the analysis significantly as data sets generated here from frozen rat brain at different PMDs were overall very similar up to 24 hr after death (Figure 1A for analysis of a 93 and 130 kb genome region; Supplemental Information).

To ensure that our data set would be a good representation of distal enhancers in the entire human brain, we focused on sampling anatomically distinct regions (Figure S1). We dissected a total of 136 regions across our donor tissues (Figure S1; Table S1). In total, 87 anatomically distinct regions were dissected, with several being sampled multiple times across different donors (Table S1). Cortical regions and subcortical nuclei of the midbrain were dissected as identified anatomically (Figure S1; Table S1). We generated 136 ChIP-seq data sets representing a combined total of 2.5 billion mapped reads (GSE40465). Technical replicate samples displayed close correlation (0.86–0.99, Supplemental Information) and were combined when needed to reach our target threshold of 8 million reads mapped per sample (Table S1; Supplemental Information).

Principal component analysis (PCA) of the separate data sets revealed a global stratification of samples based on gross anatomical location (i.e., cortex, midbrain, cerebellum [CB]) (Figure 1B; Supplemental Information). However, as anatomical sections of the brain are expected to harbor a higher degree of biological similarity to each other as compared with samples derived from different organs, the percentage of total variation due to biological variation between the data sets is relatively lower (Supplemental Information). In total, we identified ~2.9 million H3K27ac-enriched regions across all samples analyzed in the first hemisphere, ~1.4 million in the second hemisphere, and 356,747 in the additional donors. After subtracting regions overlapping known promoter regions and merging redundant enhancers between the different data sets, these corresponded to a total of 122,822: 105,558 and 87,151 nonredundant enriched regions, respectively (Figure 1C). Plotting the total number of nonredundant regions identified per hemisphere as a function of the amount of samples analyzed revealed that we sampled common H3K27ac-enriched regions in the brain almost to saturation (Figure 1D). Indeed, most enhancers were recovered from multiple samples with 45,687 enhancers being recovered from more than 10 anatomical regions (Figure 1E). A total of 83,553 promoter distal H3K27ac-enriched regions were present in at least two biological replicates (Figures 1C and 1D; Table S2). Of these, 6,829 were exclusively found in regions of the cortex (Table S3). While these distal H3K27ac-enriched regions can be considered putative enhancer elements, a number of these might still represent unannotated promoters.

Further analysis of these putative enhancers demonstrated an average size ~2.6 kb with 7,043 enhancer regions (8%) being larger than 5 kb and 731 (0.9%) exceeding 10 kb, which is reminiscent of earlier described superenhancers (Lovén et al., 2013) (Figure 1F). Several known enhancer regions in the brain were also found to be covered by the current enhancer data set (Figure 1G, shown for the *MECP2* gene; Liu and Francke, 2006), further confirming the quality of the data. For each distinct brain region analyzed, enhancer elements were recovered in at least one other sample from a different individual at an average coverage per region of ~96% (Figure 1H). As multiple data sets are added, this also results in the accumulation of enhancers that are not covered in biological replicates (Figure 1C).

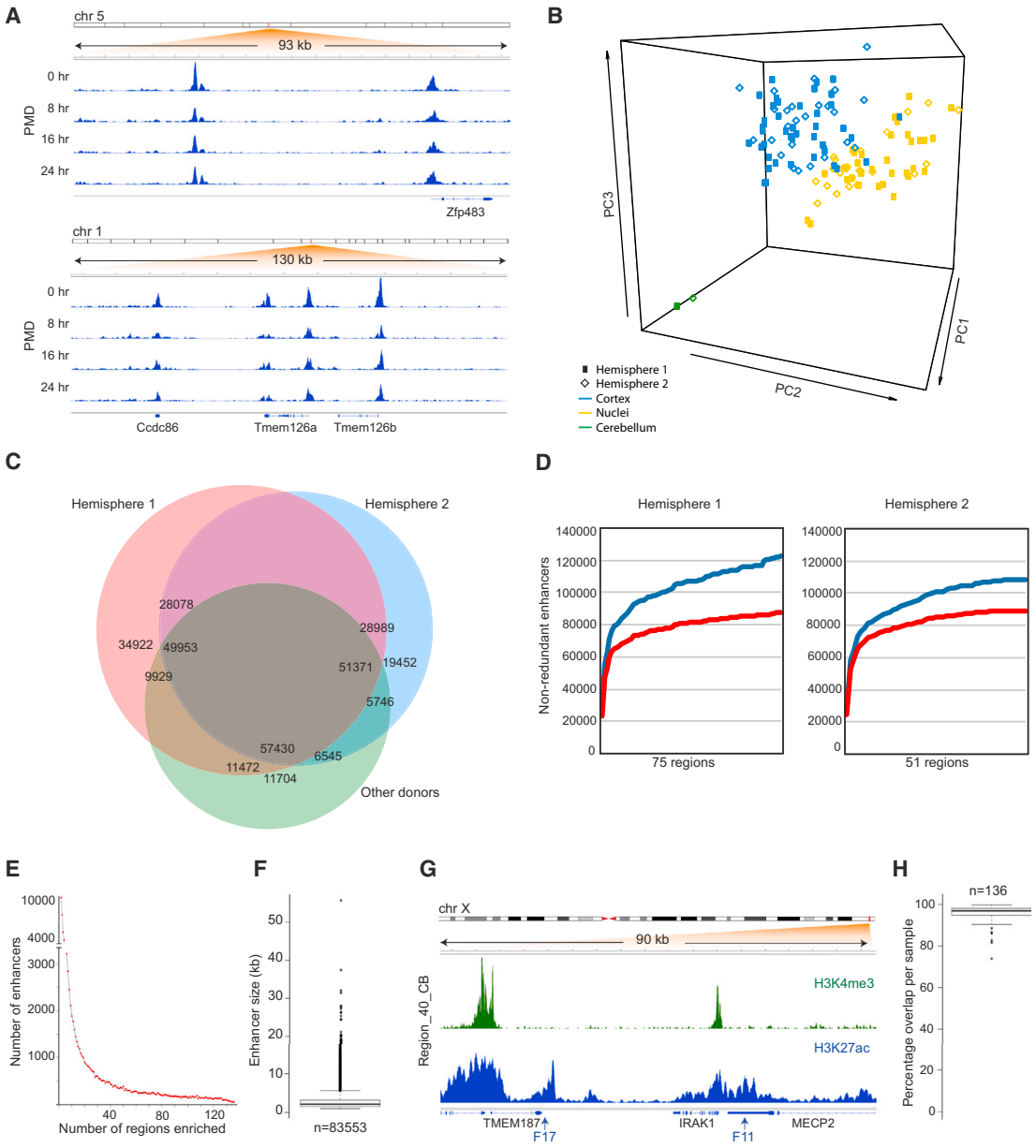

Figure 1. Promoter Distal H3K27ac-Enriched Regulatory Elements in Regions of the Human Brain

(A) H3K27ac-enriched regions in two genomic loci of whole rat brain sampled at 0, 8, 16, and 24 hr PMD. The data reveal H3K27ac-enriched regions at promoters (shown for several genes in the bottom panel) as well as at putative upstream enhancers (upper panel 5′ distal from the *ZFP483* gene) (mapped using rn4). Each track is normalized for the number of mapped reads per total million reads. Read per million normalized scale is shown ranging from 0 to 7.

(B) PCA coordinates for each sample from the two separate hemispheres. The data show overall variation based on gross anatomical location. PC1 represents 23% of variation and discriminates between CB (green) and other samples. PC2 (15% of variation) and PC3 (11% of variation) separate cortex (blue) and nuclei (yellow).

(C) Venn diagram showing total overlap of distal H3K27ac-enriched regions between hemisphere specimen 1 (red) and hemisphere 2 (blue), as well as the additional donor samples (green).

(D) Graph showing the increase in the number of unique H3K27ac-enriched regions identified per hemisphere as a function of the number of samples analyzed. Blue line depicts the enhancers identified in a single hemisphere. Red line depicts enhancers identified in biological replicates.

(E) Graph indicating the number of 83,533 enhancers enriched as a function of the number of samples they are found enriched in (total 136).

(F) Distribution of the 83,553 nonredundant enhancer sizes recovered in this study.

(G) ChIP-seq read distribution across a 70 kb region spanning the *MECP2* gene. Two tracks display enrichment for the cerebellar region (H3K4me3 in green, H3K27ac in blue). Validated enhancers are indicated (F11 and F17; Liu and Francke, 2006). The scale of the tracks runs from 0 to 7 reads per million normalized.

(H) Percentage of nonredundant enhancers per brain region that are recovered at least once in a biological replicate region analyzed in this study. Coverage for all 136 brain regions analyzed is displayed as a distribution.

See Figure S1.

These enhancers could therefore represent false positive enhancers. However, a percentage of these enhancers (35% for hemisphere 1 and 24% for hemisphere 2) was recovered from multiple samples of a single individual. Therefore, it is also possible that some of these represent interindividual variation. This is consistent with earlier reports describing the analysis of H3K27ac in different donors (Kasowski et al., 2013; Kilpinen et al., 2013; McDaniell et al., 2010; McVicker et al., 2013). Finally, our data sets closely match recently published records of H3K27ac enrichment in the brain. Strong overlap was found between the data sets described here and those previously analyzed for seven distinct brain regions (Zhu et al., 2013), as 96% of the enhancers recovered in that study was also found in the larger data set presented here. For p300 data generated from a single human fetal cortex (Visel et al., 2013), 67% was found back in these data sets. The latter was expected to be more divergent, as it involves the comparison between adult and fetal stages for which significant differences in gene expression patterns are also found (Colantuoni et al., 2011; Kang et al., 2011). Taken together, we have identified 83,533 putative enhancers, significantly expanding the compendium of putative enhancers that are found active in the human brain.

Chromatin Dynamics at Distal Enhancers Correlate with Neuronal Gene Expression Patterns in Different Regions of the Brain

To further assess the validity of the putative active enhancers identified here, we correlated their genomic position in different anatomical regions to gene expression data from matched anatomical regions. The overall genomic distribution of putative enhancers mapped in the brain was reminiscent of enhancers (Figure 2A), with preferential clustering near genes (Bernstein et al., 2012). Of the enhancers present in the intergenic regions, most (70%) were located >10 kb away from coding gene sequences, and ~22% exceeded 100 kb in distance. Using RNA sequencing data for two regions (superior temporal gyrus [STG] compared with the CB), we found that genes that are upregulated specifically in one anatomical region over another (>4-fold) were found to be more frequently associated with a close enhancer specific for the anatomical region in which the gene was upregulated (Figures 2B and 2C). This effect was primarily seen within the first 10 kb of the TSS and not for >10 kb, which is possibly due to more frequent incorrect enhancer-gene pairing at larger distances (Sanyal et al., 2012).

To further confirm a correlation between enhancer activity and gene expression in multiple anatomical regions of the brain, we calculated the Pearson correlation scores between enhancers present in a 100 kb window around the TSSs of 1,119 genes that were previously found to be differentially expressed between different regions of the brain (Hawrylycz et al., 2012) (Figure 2D; Supplemental Information). Indeed, correlation scores for enhancers that are close to these differentially regulated genes were lower compared with enhancers around nondifferentially expressed genes (Figure 2D; $p = 2.9E\text{-}5$). This confirms that enhancers in regions around differentially expressed genes show greater variability in H3K27ac enrichment.

Gene ontology (GO) analysis on genes close to enhancers in the brain confirmed that these were genes involved in neuroglial processes (Table S4), consistent with enhancers in the brain supporting neuronal gene expression networks. For instance, enhancers found in the pituitary gland were specifically associated with abnormal pituitary gland development (Table S4). However, for most neuronal functions and disorders identified, multiple anatomical regions were found to be associated, suggesting the involvement of more common inter-regional regulatory circuits.

To assess the activity of some of our putative enhancer elements experimentally, we compared our data with the VISTA enhancer database (Visel et al., 2007). This database comprises a large collection of DNA elements that were selected, based on their predicted activity as enhancers and tested in transgenic mouse assays. As an example, two of our newly identified enhancers were tested using this assay and these demonstrated reproducible staining of neural structures in E11.5 embryos, as shown in Figure 2E. We next focused on 231 DNA elements from the VISTA database selected previously by measuring ultraconservation (Visel et al., 2007) and intersected these regions with our data set. We found that ultraconserved regions that were also covered by H3K27ac in our data sets were more frequently active as an enhancer in transgenic experiments (61% compared with 50%, $p < 0.05$) (Figure 2F). Furthermore, their activity also more often localized to forebrain, midbrain, or hindbrain structures (77% versus 62%, $p < 0.05$) (Figure 2G). Collectively, these data provide strong support that our compendium of enhancers comprises bona fide enhancer sequences that support neuronal gene expression programs in the human brain.

Enhancer Patterns across Anatomical Regions in the Brain Allow the Identification of Coregulated Enhancer Networks across the Genome

A drawback of the analysis above is that the anatomical brain regions analyzed in this study are typically heterogeneous and the enhancers identified here likely have different cellular specificities within a given anatomical region. This will amplify commonalities between the different cell types within the anatomical regions such as their developmental origin and will also dilute the signal from smaller more specific sets of enhancers that are only active in select cell types or in response to external cues. This is consistent with what was found in the GO analysis for distinct anatomical samples, in which very similar GO terms were associated with data sets from different anatomical areas (Table S4). Similarly, the majority of DNA motifs identified at enhancer regions represented transcription factor binding sites that were found enriched at enhancers in most anatomical regions (Figure S2).

To identify more specific sets of enhancers (networks) that are functionally linked in a cell- or context-specific manner, we used a new strategy to analyze the data. We aligned H3K27ac-enrichment tracks from the different anatomical regions at fixed genomic positions (Figure 3A) and searched for groups of enhancers with the same enrichment profile across the brain regions (Figure 3B). We used two distinct enhancer states (i.e., enriched in a single sample or enriched in multiple samples) as viewpoints (reference enhancers) to scan the genome in order to find enhancers that were closely coregulated (showing the

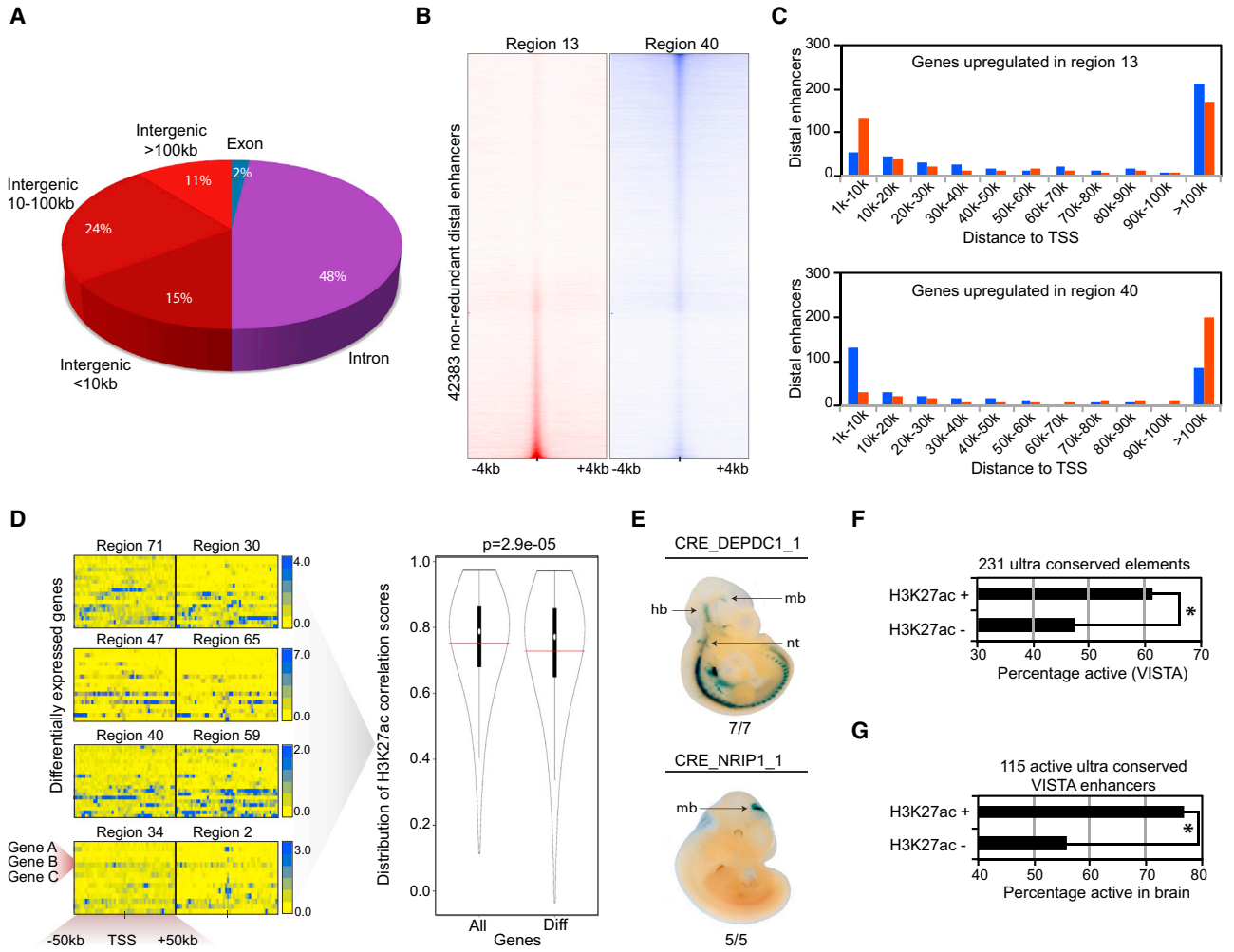

Figure 2. Chromatin Dynamics at Distal Enhancers Correlate with Neuronal Gene Expression Patterns

(A) Distribution of identified promoter distal H3K27ac-enriched regions shared between replicates across the genome.

(B) Heatmap of putative enhancers shared between or specific to the STG (Region_13_STGm, red) and CB (Region_40_CB, blue) for segments of 8 kb surrounding enhancers. Both colors represent H3K27ac-enrichment reads normalized per million.

(C) Graphs based on genes upregulated at least 4-fold with a q value of 1E-5 in Region_13_STGm (upper graph) over Region_40_CB or vice versa (lower graph). The closest distal elements found near these gene promoters are counted for both Region 40 (blue bars) and Region 13 (red bars) and allocated to different distance intervals shown on the x axis.

(D) Four examples of comparisons between two given anatomical regions for differentially expressed genes between those regions (Hawrylycz et al., 2012). For each region (in pairs), the level of H3K27ac enrichment (from low/yellow to high/blue) is shown (displaying 100 kb sequence centered at TSSs). Scale bars indicate read count normalized per million reads. Comparisons in the violin plot were done by calculating a Pearson correlation score for each enhancer between all data sets based on quantile normalized counts in a 2 kb window around the center of the enhancer. The violin plot shows the distribution of correlations found for all enhancers across all samples. (All) compared with those found within 100 kb of a differentially expressed gene across all samples (Diff). Dissimilarity between distributions was calculated using a Mann-Whitney U test.

(E) Two transgenic mice at E11.5 showing enhancer-driven expression of a LacZ reporter construct in neuronal structures.

(F) The top graph indicates comparison of the human enhancer data set generated here to 231 ultraconserved elements that were tested in the same transgenic assay and deposited in the VISTA enhancer database by others (Visel et al., 2007). The percentage of enhancers with activity in transgenic animals is shown for conserved elements that overlap H3K27ac in the brain (n = 49) versus those that do not.

(G) The same analysis is shown for 115 ultraconserved elements that were active in transgenic animals as a function of the percentage that was active in forebrain, midbrain, or hindbrain. Cumulative probabilities of the differences seen in both graphs are indicated (*$p < 0.05$).

Also see Figure S2.

same pattern of enrichment across samples). We identified distinct groups of coregulated enhancers for both separate states. For instance, two viewpoint enhancers that were enriched in multiple samples yielded 495 and 442 coregulated enhancers (Figures 3C and 3D). In contrast to the analysis of the whole data set, these smaller networks were associated with very specific gene functions, supporting either neuronal or glial cell states (Figures 3C and 3D). Similarly, using an enhancer

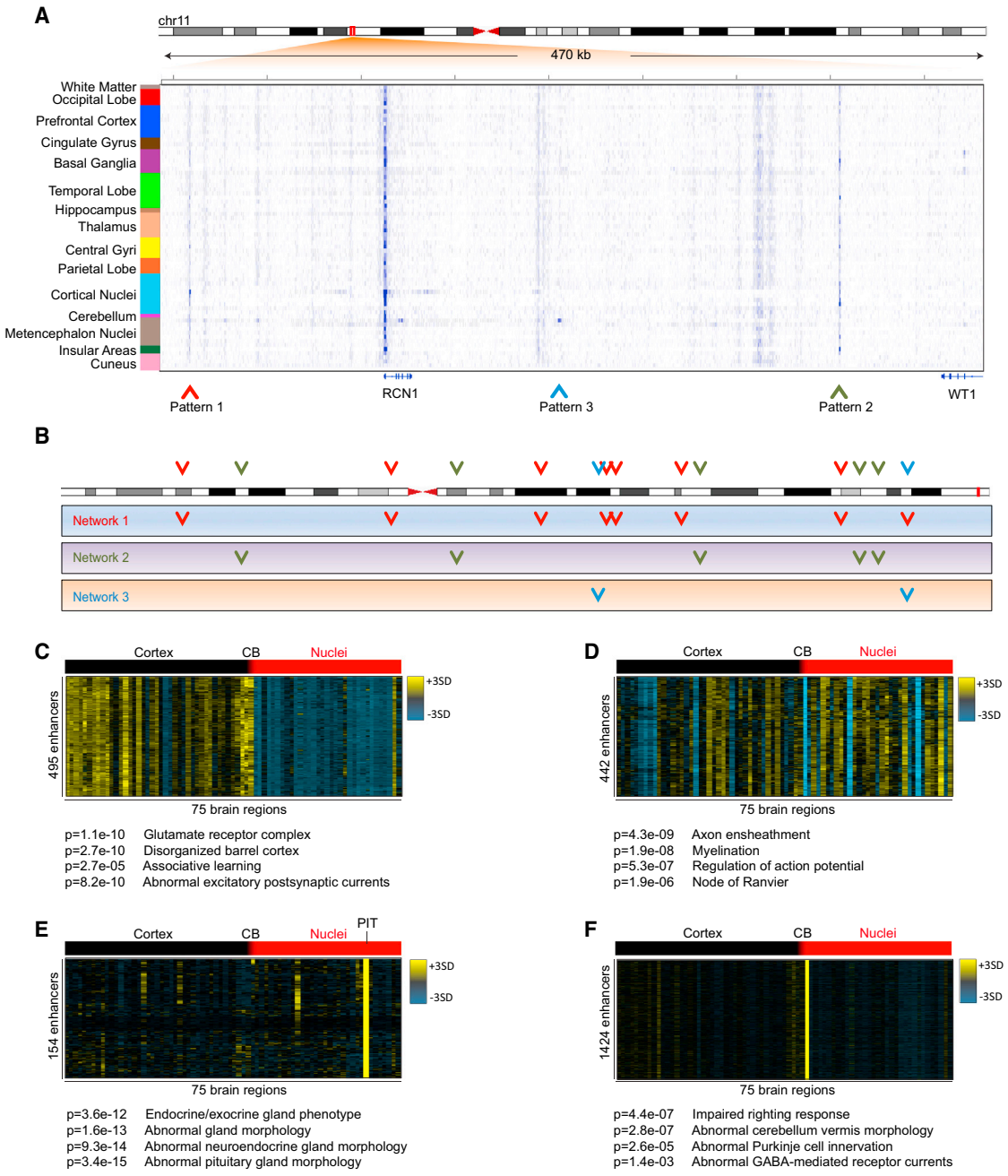

Figure 3. Enhancer Patterns across Anatomical Regions in the Brain Allow the Identification of Coregulated Enhancer Networks across the Genome

(A) H3K27ac-enrichment tracks for all regions from hemisphere 1 merged into one heatmap for a 470 kb segment overlapping the RCN1 and WT1 genes. Several putative enhancers are present, three of which are indicated by arrows and show a distinct pattern of enrichment across all samples.

(B) Cartoon indicating how distinct networks of enhancers can be extracted from heterogeneous samples by considering coregulation across the genome.

(C–F) H3K27ac-enrichment patterns *Z* score normalized across 75 ChIP-seq samples derived from a single hemisphere ordered in a fixed position. Samples are ordered vertically. Each horizontal line is an enhancer that correlates with the viewpoint enhancer. The color scale (yellow to blue) ranges 3 SDs above and below the mean enrichment (black) over the 75 regions per single genomic region. The number of lines (enhancer regions) is (C) n = 495 with 0.83 mean correlation, (D) n = 442 with 0.76 mean correlation, (E) n = 154 with 0.90 mean correlation, and (F) n = 1424 with 0.90 mean correlation. Distinct network functions are derived using GREAT analysis and are shown for each coregulated enhancer set

Also see Figure S3.

enriched selectively in the pituitary gland or CB as a viewpoint yielded coregulated enhancers (Figures 3E and 3F) that were also found selectively enriched in these regions. These two networks were specifically linked to genes that function in pituitary and cerebellar specific processes. This demonstrates that coregulated enhancers can be identified and grouped into specific networks using both single sample-enriched as well as multiple sample-enriched enhancer states as a viewpoint (Figures 3E and 3F). Using this analysis for an enhancer selectively enriched in the pineal gland, we identified 334 enhancers that were enriched for the CRX transcription factor binding site, which is a master regulator of pineal specific gene expression patterns (Figure S3) (Rovsing et al., 2011). Thus, our analysis of coregulated enhancer networks over a large number of brain regions allows us to substantially increase the resolution of enhancer analysis in heterogeneous tissue compared with the analysis of single data sets.

Global Network Analysis Identifies Distinct Enhancer Modules in the Human Brain

To get a sense of the total amount of networks active in the human brain, we employed a more global analysis that was not dependent on the prior selection of viewpoint enhancers. The total number of networks in the brain is both a function of the minimal correlation score used between its resident enhancers as well as the minimal number of enhancers allowed in the network (network size; Figure S4A). Further analysis showed that 77.08% of all enhancers was in a network of at least 100 or more enhancers following a minimal correlation threshold of 0.7 and using each individual enhancer as a separate viewpoint (Figure S4A). This resulted in a fraction of enhancers appearing in multiple networks potentially indicating clusters of enhancers active in more than one network (multimodal enhancers; Figures S4B–S4D). To assign enhancers into separate networks, we correlated all enhancers to each other and used a dynamic tree cutting algorithm (Langfelder et al., 2008) to identify distinct coregulated enhancer networks on a global scale (Figure 4A). While providing a more global overview of the networks present in the brain, the disadvantage of this approach is that it ignores the biological implications of overlap between the different networks (Figure S4), as these could represent clusters of different enhancers.

Two hundred eighty-eight distinct coregulated enhancer networks were identified with a size of between 100 and 865 enhancers (average enhancer content 228; Figure 4B). With this analysis, 93% of all enhancers could be placed in separate modules, while a total of 5,177 enhancers was not assigned. These coregulated enhancer networks could again be linked to very distinct gene functions that represented specific neuronal processes such as shown for module 280, 14 (Figures 4C and 4D), and many other examples (Table S5). In addition, context-specific modules were also found such as those involved in tissue responses to external cues. For instance, module 34 was linked to hypoxia-related processes consistent with our samples being derived from a recently deceased brain (Figure 4E), whereas module 200 was clearly linked to immune responses and inflammatory processes that could be associated with activity in microglial cells of the brain (Figure 4F). Therefore, many of these networks could represent cell type-specific information within a heterogeneous tissue sample.

This functional variation between networks was also reflected in the diversity of transcription factor binding motifs found at the H3K27ac-enriched regions comprising a single module (Figure S4E). This is consistent with distinct transcription factors governing the activity of specific enhancer sets in response to external cues. Notably, enhancer networks linked to genes involved in diseases of the brain, such as schizophrenia, were also linked to synaptic transmission (Figure 4C). Similarly networks linked to cancers of the brain were also associated with developmental processes in the early embryo (Figure 4D). As over 85% of polymorphisms that associate with altered disease susceptibility occur in introns or intergenic regions of the genome, enhancers in such networks likely account for the association between noncoding elements and disease susceptibility (Bernstein et al., 2012; Maurano et al., 2012; Ward and Kellis, 2012). This suggests that SNPs at enhancers potentially affect gene expression in an organ-specific fashion, leading to specific disease phenotypes.

Noncoding PD-Associated SNPs in the PARK16 and α-Synuclein Loci Alter Transcription Factor Binding Sites at Enhancers in the Human Brain

To determine whether we could identify disease associated variations at candidate enhancers in the human brain, we focused on the neurodegenerative disorder PD. To demonstrate the preferential association between PD-associated SNPs and enhancer sequences detected in the brain, H3K27ac-enriched enhancer regions were compared with SNPs from the HaploReg genome-wide association database (Ward and Kellis, 2012). Nine unrelated cell types were used as a control (Ernst et al., 2011). Overall, enhancer data sets represent a similar number of distal enriched regions, with 107,407 nonredundant putative enhancers in the nine cell types compared with 122,882 and 105,558 regions identified in each hemisphere separately. When comparing the percentage of SNPs associated with PD located within enhancers, given as a function of their significance, we observed an overrepresentation of highly significant SNPs located in enhancer sequences from both brain specimens compared with the nine control cell types (Figure 5A). This correlation was specific to the brain and not recovered when comparing SNPs associated with other traits not directly related to this organ (heart failure, obesity). No single brain region had significantly more PD-associated SNPs located within H3K27ac-enriched sequences, consistent with PD globally affecting many brain regions and individual neuronal types (Mattson and Magnus, 2006). Importantly, putative enhancer sequences were found in genetic loci spanning major PD-associated polymorphisms, including the PARK16 locus and a locus containing the *α-synuclein* (*SNCA*) gene, which is mutated in familial cases of PD (Satake et al., 2009; Simón-Sánchez et al., 2009). In both cases, the associated SNPs appear in noncoding sequences, and their functional relevance for differential susceptibility to PD is not yet understood.

The α-synuclein locus contains some of the most significant PD-associated SNPs (Satake et al., 2009; Simón-Sánchez et al., 2009), two of which were identified in separate population

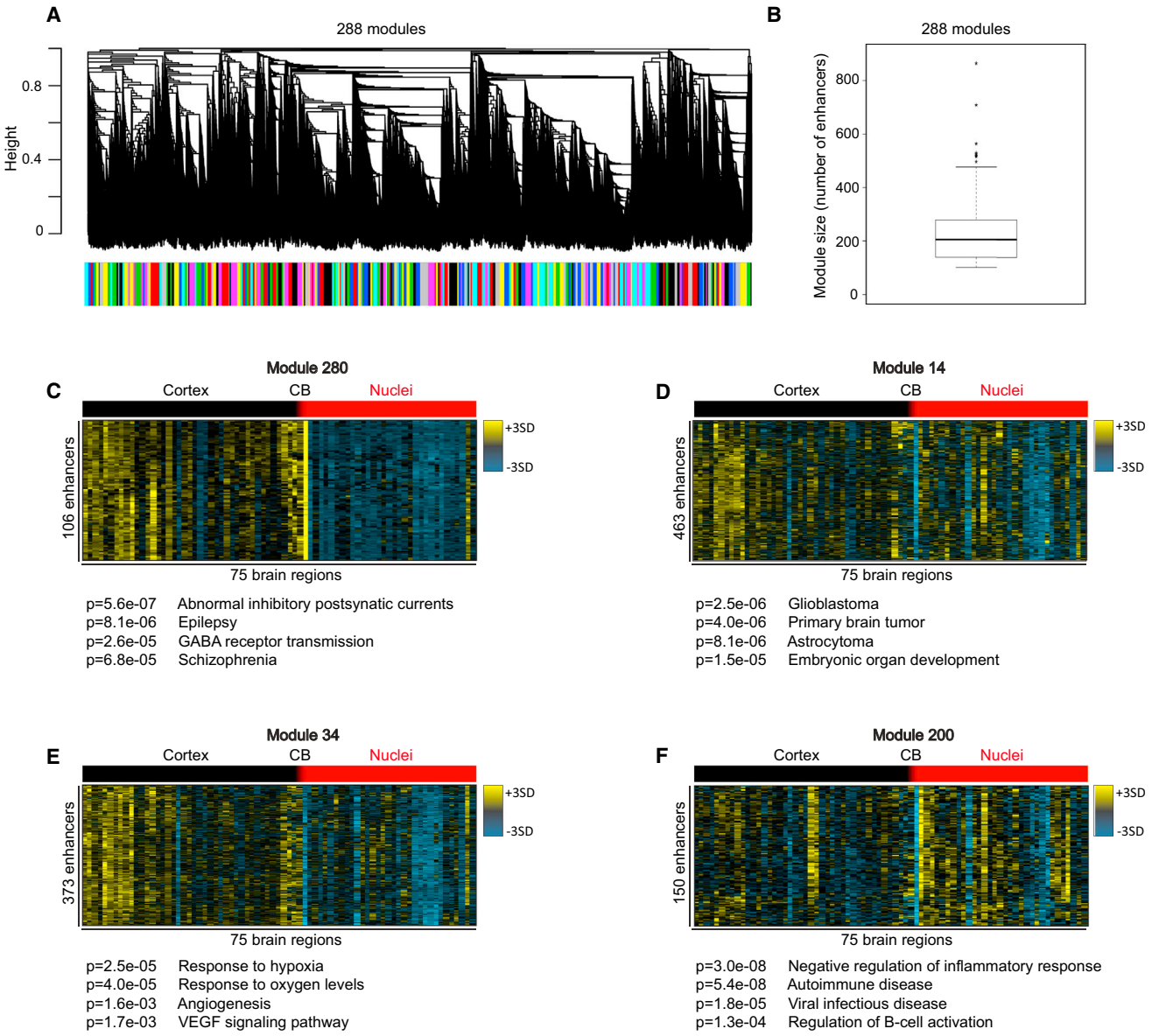

Figure 4. Global Network Analysis Identifies 288 Distinct Enhancer Modules in the Human Brain

(A) Assignment of enhancers to separate modules using average linkage followed by a dynamic tree-cutting algorithm (Langfelder et al., 2008).

(B) Boxplot showing the distribution of module sizes bases on the number of enhancers present in each module.

(C–F) Single modules derived from the dynamic tree-cutting algorithm in (A) showing H3K27ac-enrichment patterns *Z* score normalized across 75 ChIP-seq samples from hemisphere 1 ordered in a fixed position. Samples are ordered vertically. Each horizontal line is an enhancer that was assigned to the indicated module. The color scale (yellow to blue) ranges 3 SDs above and below the mean enrichment (black) over 75 regions per single genomic region. A selection of functional annotations for genes linked to enhancers in a module is shown below each module. Enhancer-gene links were determined using GREAT (McLean et al., 2010).

Also see Figure S4.

studies (one of Japanese ancestry and one of European). These span a 50 kb haplotype block on the distal half of the gene (Figure 5B, red arrows) (http://www.hapmap.org). Within this chromosomal segment, two SNPs are found 20 bp apart at a putative enhancer, with each appearing to be in perfect linkage disequilibrium (LD = 1) with the disease-associated SNPs of matching minor allele frequency derived from the two studies (Figure 5B, purple arrow). Hence, while not corresponding to SNPs present on the array, this represents a clear association between sequence alterations within a putative enhancer and increased PD incidence.

To demonstrate that this region can function as an enhancer in vivo, we generated transgenic mice for this enhancer using a LacZ reporter construct (Visel et al., 2007). Reproducible LacZ

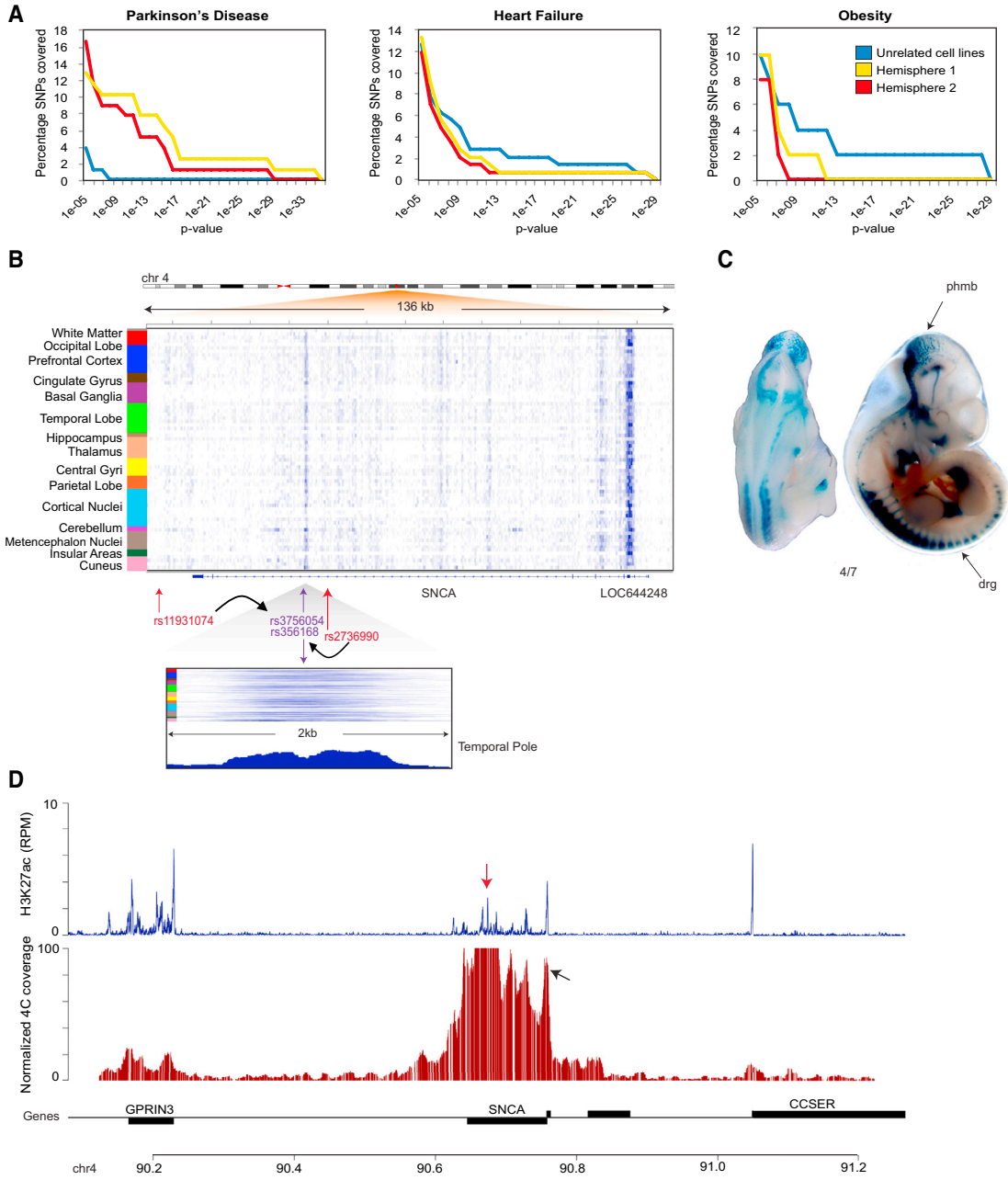

Figure 5. Association between *cis*-Regulatory DNA Elements and PD-Associated SNPs

(A) Percentage of SNPs associated with each disorder (as a function of their respective p value) is represented for SNPs mapping to enhancer sequences found in either nine unrelated cell lines (blue line) or the two hemispheres examined (red and yellow line).

(B) H3K27ac-enrichment tracks for all regions from brain 1 merged into one heatmap for a 140 kb region spanning the *SNCA* gene. Two different SNPs were found in separate studies as influencing PD incidence (red arrows). For each disease-associated SNP found on the genotyping array, an additional SNP can be found in perfect LD (LD = 1, purple arrows), both of which (rs3756054 and rs356168, 20 bp apart) also overlap a single putative enhancer region. An inset below shows the location of the SNP at higher resolution (2 kb) for all tracks (heatmap), being at the center of the enriched region). The bottom track of the inset (peaks) shows as an example H3K27ac enrichment in the temporal pole (range, 0–3 reads per million normalized).

(C) Transgenic mouse at E11.5 showing reproducible SNCA enhancer driven LacZ expression in posterior hindbrain and midbrain boundary (phmb) and dorsal root ganglion (drg) (4/7).

(D) Track showing 1 Mb around the *SNCA* gene showing chromosome conformation capture results using the SNCA enhancer as a viewpoint (bottom panel in red). The large peak shows enrichment at the viewpoint (viewpoint enhancer indicated by red arrow above H3K27ac panel). Enrichment at other regions demonstrates looping of the viewpoint to those regions such as the SNCA promoter (black arrowhead) as well as the *GPRIN3* and *CCSER* genes. H3K27ac enrichment is shown in blue above the 4C tracks. Genes (black boxes) are at the bottom of the panel (biological replicate 4C for hemisphere 2).

See Figure S5.

staining of the hindbrain and midbrain boundary and dorsal root ganglion was seen, consistent with the human sequence acting as an enhancer (Figure 5C). As moderate alteration of *α-synuclein* expression leads to familial PD with high penetrance (Stefanis, 2012), these data suggest that variations at this particular enhancer sequence in the brain could explain the association with PD incidence.

To further confirm that this region functions as an enhancer in the human brain, as well as to identify its target gene(s), we performed chromosome confirmation capture combined with sequencing (4C-Seq) analysis (van de Werken et al., 2012) using the putative *α-synuclein* enhancer as a viewpoint. This technique identifies genomic locations with which the viewpoint is physically connecting. As enhancers function by looping to their target promoters, this method therefore represents a measure of in vivo enhancer activity as well as a method to identify their target genes. A robust interaction between the enhancer and the *α-synuclein* promoter region was observed (Figures 5D and S5) demonstrating that the enhancer forms a loop to its presumed target promoter in a relevant environment. A second interaction of the enhancer with *GPRIN3*, a nearby gene that is a subunit of the NMDA glutamate receptor complex was also observed. Interestingly, these receptors are considered potential therapeutic targets for the disease (Johnson et al., 2009), raising the possibility that in addition to *SNCA*, variations in the regulation of this gene are also involved in altered disease susceptibility to PD.

In contrast to the *SNCA* enhancer that is enriched for H3K27ac in multiple regions throughout the brain, we found that the enhancer in the PARK16 locus, covering the most significant disease-associated SNP, was more selectively active in the CB (Figure 6A). Interestingly, the CB is currently gaining attention as being structurally altered and directly involved in the pathophysiology of PD (Wu and Hallett, 2013). Analysis of this sequence in transgenic mice confirmed reproducible staining of midbrain and neural tube consistent with the human sequence acting as an enhancer element (Figure 6B).

Recent work has demonstrated that deficiency of the *RAB7L1* gene, which is one of the genes in the PARK16 locus, can lead to neurodegeneration similar to mouse models of PD (MacLeod et al., 2013), and thus, this gene was believed to contribute to the association between PD and this locus. In order to determine whether the enhancer associated to the PARK16 locus directly explains this by regulating the *RAB7L1* gene, we performed 4C-Seq analysis using the PARK16 enhancer sequence as a viewpoint in human CB. The analysis demonstrated no clear evidence for looping between the enhancer and the promoter of the *RAB7L1* gene. However, the resolution of the 4C analysis also does not exclude its involvement. We did find interactions with several other distal genes, some of which have been similarly implicated in neuronal degeneration but are located further away (Figure 6C). For example, *MK2* (*MAPKAPK2*) promotes neurodegeneration in PD models (Thomas et al., 2008). This suggests that the activity of this enhancer is much more complex than the regulation of a single gene. Altogether, with 53 PD-associated SNPs being covered by enhancers in the brain (Table S6), these results demonstrate that genomic variations within enhancer sequences could collectively explain variable susceptibility to PD in the human population by differentially regulating either specific or larger sets of genes. Furthermore, we demonstrate how these can be identified using the data sets generated in this study.

DISCUSSION

While gene expression analysis specifies active and inactive genes, mapping the epigenome provides important complementary information by explaining why certain genes are active or inactive and which genes have the potential to become activated in response to external cues. Furthermore, it allows the identification of the genomic elements responsible for this regulation on a large scale as well as the identification of the master regulatory factors that control these genomic elements. In this work, we have generated a large data set that allows the annotation of *cis*-regulatory genomic elements in different regions of the human brain. Given the diversity of neuronal subtypes in the brain and the plethora of signals a cell needs to be poised to respond to, regional variation in enhancer patterns reflects both changes in cellular heterogeneity in distinct anatomical regions, as well as technical variation inherent to ChIP-Sec. This generates noise that complicates the regional interpretation of specific sets of enhancers within complex heterogeneous tissues such as the brain. This noise is less obvious when comparing the global epigenetic state of tissues that are biologically distinct (i.e., whole liver and muscle), as it will uncover the common developmental features of its resident cells (Creyghton et al., 2010; Zhu et al., 2013). However, within a complex tissue with a high degree of biological similarity and a fair amount of heterogeneity, the distillation of select enhancer networks that follow specialized functions has been problematic.

Using these variations as an advantage, we show how the analysis of enhancer patterns across many anatomical regions of the brain can lead to the identification of coregulated enhancer networks that appear functionally distinct. These networks might in some cases represent cell type-specific enhancer networks but can also represent common enhancer networks used by several neuronal subtypes throughout the brain. The distinction between separate networks is of particular importance, as even single cell types contain separate functional networks that regulate the diverse cellular responses to external cues. These typically stay hidden in global analyses, especially when using homogeneous culture systems. These context-specific networks that are activated in response to external cues can either be regionalized or more widespread in nature, such as those involved in modulating responses to hypoxia or infection. Thus, analyzing coregulation significantly increases the resolution at which enhancers in complex tissues can be annotated and represents an important step to uncover the complexity of enhancer networks within the brain.

Additionally, these data, in contrast to gene expression studies, are particularly useful for understanding the persistent correlation between noncoding regions in the genome and disease susceptibility. As such, we find indications of the involvement of noncoding genomic alterations at putative enhancer elements associated with increased susceptibility to PD, including a new enhancer at the α-synuclein gene, which is found mutated in familial forms of PD. We demonstrate that enhancers

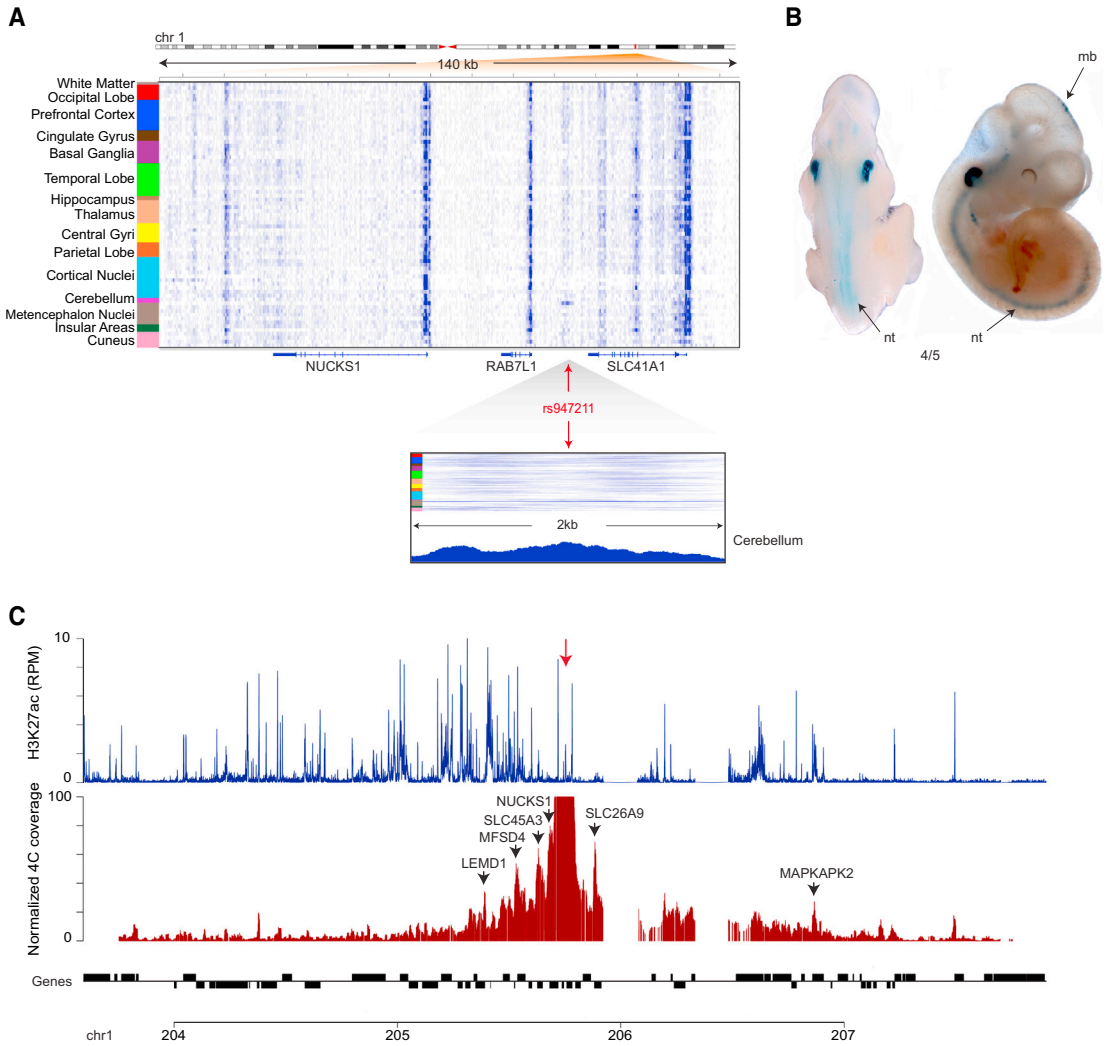

Figure 6. Association between a *cis*-Regulatory DNA Element in CB and a PD-Associated SNP in the PARK16 Locus

(A) H3K27ac-enrichment tracks merged into one heatmap where color intensities per lane represent the intensity of the peaks in each sample (both hemispheres). A 140 kb region is shown for the PARK16 locus, where H3K27ac-enriched regions and position of a PD-associated SNP (red arrow) are represented. An inset below shows the location of the SNP at higher resolution (2 kb) for all tracks (heatmap), being at the center of the enriched region. The bottom track of the inset (peaks) shows as an example H3K27ac-enrichment in the CB (range, 0–5 reads per million normalized).

(B) Transgenic mouse at E11.5 showing reproducible PARK16 enhancer driven LacZ expression in midbrain and neural tube (4/5).

(C) Track showing 4 Mb around the PARK16 locus showing chromosome conformation captures results using the PARK16 enhancer as a viewpoint (bottom panel in red). The large peak shows enrichment at the viewpoint (viewpoint enhancer indicated by red arrow above H3K27ac panel). Enrichment at other regions demonstrates looping of the viewpoint to those regions (black arrows). H3K27ac enrichment is shown in blue above the 4C tracks. Genes (black boxes) are at the bottom (zoom in for viewpoint for both biological replicates, see Figure S6).

at PD associated SNPs can either be active in many anatomical regions as shown for *SNCA* or in more specific regions such as shown for the PARK16 locus. This emphasizes the importance of investigating these enhancer variations in a relevant biological context. We demonstrate how our analysis leads to the identification of potential target genes by using these distal regulatory elements for chromosome confirmation capture in postmortem tissue. With multiple PD-associated SNPs occurring in enhancers in the brain, these data suggest that fluctuations in the expression of several genes, caused by variations at multiple enhancers, collectively set the stage for PD penetrance.

Following the identification of a large portion of the noncoding regulatory elements in the brain, it will now be possible to employ large-scale chromatin conformation assays to pair enhancer regions to their correct target promoters. This will be crucial to generate a complete picture of the gene regulatory landscape, as many enhancers are regulating genes that are not their nearest neighbor (Sanyal et al., 2012). In this light, it will be important to correctly match anatomical and functional regions of the brain between different data sets from different studies and to account for interindividual variations. Furthermore, it will be important to start to ascertain the role of enhancers in the regulation of

gene expression networks the brain in the context of single cell types. Analyzing enhancers by coregulation might represent a step in this direction. As more specimens are processed, these experiments pave the way toward a full understanding of the epigenetic complexity of the human brain.

EXPERIMENTAL PROCEDURES

Full methods accompany this paper (Supplemental Information). Briefly, two adult nondemented control female human hemispheres were obtained from the Netherlands Brain Bank (http://www.brainbank.nl/) as well as several separate regions stemming from different donors (Table S1; Supplemental Information). Informed consent was acquired meeting all ethical and legal requirements for autopsy, tissue storage, and use of tissue and clinical data for research. Tissue was flash frozen in liquid nitrogen and stored at −80°C. Neuropathological examination revealed no significant abnormalities in either specimen, although partial age-related neuronal atrophy is more likely to have occurred in specimen 2 given the advanced age (Supplemental Information). Frozen tissue was dissected at −20°C, added to precooled DAG medium (phenol-red free Dulbecco's modified Eagle's medium [Gibco] and BSA 1 g per 0.5 L) and immediately homogenized on ice using a cold 2 ml Dounce homogenizer. This was followed by chemical crosslinking using a 10× crosslinking solution containing 11% formaldehyde (Supplemental Information). Samples were further processed for ChIP-seq as described previously (Creyghton et al., 2010; Supplemental Information) using the following antibodies: H3K4me3 (07-473) and abcam H3K27ac (ab4729) (Millipore/Upstate). Shearing was done on the Covaris S Series sonicator. Samples for Solexa sequencing were run using the HiSeq 2000 genome sequencer (SCS v.2.6, pipeline 1.5) at the MIT BioMicroCenter. SOLiD based sequencing was done on the SOLiD 5500 xl and xlw genome sequencers (http://ngs.hubrecht.eu/).

Sequences were aligned using Bowtie software on the murine (mm9), rat (rn4), and human (hg19) genomes (https://www.genome.ucsc.edu), excluding reads with either more than one mismatch (three for color space) or with multiple alignments. Reads that had more than two exact matches were also excluded to correct for sequence bias. For all entered samples, between 8 to 20 million reads were successfully mapped in order to be included in data sets, and fragment in peak (FRiP) scores all well exceeded the 1% threshold used by ENCODE (Table S1; Landt et al., 2012). Statistically significant enriched regions for H3K27ac were identified using MACS2 v.2.0.8. Whole-cell extract controls were generated for a number of regions but not used in the analysis since the internal lambda control from the MACS algorithm proved a more stringent correction (see Supplemental Information). Animal experiments were approved by the Animal Experiments Committee (Dier Experimenten Commissie [DEC]).

Enhancer Network Analysis

Enhancer tracks for all regions analyzed in hemisphere 1 were ordered in a fixed position grouping cortical and noncortical regions together. Each single enhancer was *Z* score normalized to indicate variation from the mean enrichment score across all regions for the enhancer analyzed. The resulting sequence of enrichment across the region was compared with that of all other enhancer regions using the same fixed order of individual anatomical regions. Pearson correlations between all enhancer pairs were calculated and used for network identification. Viewpoint enhancers were manually selected, and coregulated enhancers were identified at a selected correlation cutoff. This analysis was then repeated in the second hemisphere, and only enhancers that correlated in both hemispheres analyzed separately were admitted to the network. For global network analysis, Pearson correlations identified above were allocated to a matrix containing all ~5 billion correlations. The matrix was then clustered using average linkage, and separate modules were identified using a dynamic tree cutting algorithm (Langfelder et al., 2008).

ACCESSION NUMBERS

The data discussed in this publication have been deposited in National Center for Biotechnology Center's Gene Expression Omnibus (GEO) and are accessible through GEO Series accession number http://www.ncbi.nlm.nih.gov/geo/query/acc.cgi?acc=GSE40465.

SUPPLEMENTAL INFORMATION

Supplemental Information includes Supplemental Experimental Procedures, six figures, and six tables and can be found with this article online at http://dx.doi.org/10.1016/j.celrep.2014.09.023.

AUTHOR CONTRIBUTIONS

M.P.C., M.W.V., and P.R. conceived and designed the experiments. M.P.C., M.W.V., P.R., P.M.C., and G.G. analyzed the data. M.W.V., P.R., J.K., E.B., O.B., P.W.T., N.L., C.M., and S.H. performed the experiments. H.C., W.L., E.C., and M.P.C. supervised experiments and analyses. H.C., W.L., E.C., and N.B.B. contributed critical resources. M.P.C., M.W.V., and P.R. wrote the manuscript.

ACKNOWLEDGMENTS

We thank Stuart Levine at the MIT Bio Micro Center for managing the SOLEXA pipeline; Len Pennacchio for the HSP68-LacZ constructs; and Catherine Rabouille, Thijn Brummelkamp, and Helen Pickersgill for critical reading of the manuscript. This work was funded by the Dutch Royal Academy of Sciences (KNAW), the Dutch Cancer Foundation (KWF) grant HUBR2012-5392, and Parkinson's Foundation (Stichting ParkinsonFonds).

Received: March 27, 2014
Revised: June 26, 2014
Accepted: September 12, 2014
Published: October 16, 2014

REFERENCES

Andersson, R., Gebhard, C., Miguel-Escalada, I., Hoof, I., Bornholdt, J., Boyd, M., Chen, Y., Zhao, X., Schmidl, C., Suzuki, T., et al.; FANTOM Consortium (2014). An atlas of active enhancers across human cell types and tissues. Nature *507*, 455–461.

Baylin, S.B., and Ohm, J.E. (2006). Epigenetic gene silencing in cancer-a mechanism for early oncogenic pathway addiction? Nat. Rev. Cancer *6*, 107–116.

Bernstein, B.E., Mikkelsen, T.S., Xie, X., Kamal, M., Huebert, D.J., Cuff, J., Fry, B., Meissner, A., Wernig, M., Plath, K., et al. (2006). A bivalent chromatin structure marks key developmental genes in embryonic stem cells. Cell *125*, 315–326.

Bernstein, B.E., Birney, E., Dunham, I., Green, E.D., Gunter, C., and Snyder, M.; ENCODE Project Consortium (2012). An integrated encyclopedia of DNA elements in the human genome. Nature *489*, 57–74.

Bulger, M., and Groudine, M. (2011). Functional and mechanistic diversity of distal transcription enhancers. Cell *144*, 327–339.

Colantuoni, C., Lipska, B.K., Ye, T., Hyde, T.M., Tao, R., Leek, J.T., Colantuoni, E.A., Elkahloun, A.G., Herman, M.M., Weinberger, D.R., and Kleinman, J.E. (2011). Temporal dynamics and genetic control of transcription in the human prefrontal cortex. Nature *478*, 519–523.

Creyghton, M.P., Cheng, A.W., Welstead, G.G., Kooistra, T., Carey, B.W., Steine, E.J., Hanna, J., Lodato, M.A., Frampton, G.M., Sharp, P.A., et al. (2010). Histone H3K27ac separates active from poised enhancers and predicts developmental state. Proc. Natl. Acad. Sci. USA *107*, 21931–21936.

Dulac, C. (2010). Brain function and chromatin plasticity. Nature *465*, 728–735.

Ernst, J., Kheradpour, P., Mikkelsen, T.S., Shoresh, N., Ward, L.D., Epstein, C.B., Zhang, X., Wang, L., Issner, R., Coyne, M., et al. (2011). Mapping and analysis of chromatin state dynamics in nine human cell types. Nature *473*, 43–49.

Hawrylycz, M.J., Lein, E.S., Guillozet-Bongaarts, A.L., Shen, E.H., Ng, L., Miller, J.A., van de Lagemaat, L.N., Smith, K.A., Ebbert, A., Riley, Z.L., et al. (2012). An anatomically comprehensive atlas of the adult human brain transcriptome. Nature *489*, 391–399.

Heintzman, N.D., Hon, G.C., Hawkins, R.D., Kheradpour, P., Stark, A., Harp, L.F., Ye, Z., Lee, L.K., Stuart, R.K., Ching, C.W., et al. (2009). Histone modifications at human enhancers reflect global cell-type-specific gene expression. Nature *459*, 108–112.

Johnson, K.A., Conn, P.J., and Niswender, C.M. (2009). Glutamate receptors as therapeutic targets for Parkinson's disease. CNS Neurol. Disord. Drug Targets *8*, 475–491.

Kang, H.J., Kawasawa, Y.I., Cheng, F., Zhu, Y., Xu, X., Li, M., Sousa, A.M., Pletikos, M., Meyer, K.A., Sedmak, G., et al. (2011). Spatio-temporal transcriptome of the human brain. Nature *478*, 483–489.

Kasowski, M., Kyriazopoulou-Panagiotopoulou, S., Grubert, F., Zaugg, J.B., Kundaje, A., Liu, Y., Boyle, A.P., Zhang, Q.C., Zakharia, F., Spacek, D.V., et al. (2013). Extensive variation in chromatin states across humans. Science *342*, 750–752.

Kilpinen, H., Waszak, S.M., Gschwind, A.R., Raghav, S.K., Witwicki, R.M., Orioli, A., Migliavacca, E., Wiederkehr, M., Gutierrez-Arcelus, M., Panousis, N.I., et al. (2013). Coordinated effects of sequence variation on DNA binding, chromatin structure, and transcription. Science *342*, 744–747.

Konopka, G., and Geschwind, D.H. (2010). Human brain evolution: harnessing the genomics (r)evolution to link genes, cognition, and behavior. Neuron *68*, 231–244.

Landt, S.G., Marinov, G.K., Kundaje, A., Kheradpour, P., Pauli, F., Batzoglou, S., Bernstein, B.E., Bickel, P., Brown, J.B., Cayting, P., et al. (2012). ChIP-seq guidelines and practices of the ENCODE and modENCODE consortia. Genome Res. *22*, 1813–1831.

Langfelder, P., Zhang, B., and Horvath, S. (2008). Defining clusters from a hierarchical cluster tree: the Dynamic Tree Cut package for R. Bioinformatics *24*, 719–720.

Liu, J., and Francke, U. (2006). Identification of cis-regulatory elements for MECP2 expression. Hum. Mol. Genet. *15*, 1769–1782.

Lovén, J., Hoke, H.A., Lin, C.Y., Lau, A., Orlando, D.A., Vakoc, C.R., Bradner, J.E., Lee, T.I., and Young, R.A. (2013). Selective inhibition of tumor oncogenes by disruption of super-enhancers. Cell *153*, 320–334.

MacLeod, D.A., Rhinn, H., Kuwahara, T., Zolin, A., Di Paolo, G., McCabe, B.D., Marder, K.S., Honig, L.S., Clark, L.N., Small, S.A., and Abeliovich, A. (2013). RAB7L1 interacts with LRRK2 to modify intraneuronal protein sorting and Parkinson's disease risk. Neuron *77*, 425–439.

Maston, G.A., Evans, S.K., and Green, M.R. (2006). Transcriptional regulatory elements in the human genome. Annu. Rev. Genomics Hum. Genet. *7*, 29–59.

Mattson, M.P., and Magnus, T. (2006). Ageing and neuronal vulnerability. Nat. Rev. Neurosci. *7*, 278–294.

Maurano, M.T., Humbert, R., Rynes, E., Thurman, R.E., Haugen, E., Wang, H., Reynolds, A.P., Sandstrom, R., Qu, H., Brody, J., et al. (2012). Systematic localization of common disease-associated variation in regulatory DNA. Science *337*, 1190–1195.

McDaniell, R., Lee, B.K., Song, L., Liu, Z., Boyle, A.P., Erdos, M.R., Scott, L.J., Morken, M.A., Kucera, K.S., Battenhouse, A., et al. (2010). Heritable individual-specific and allele-specific chromatin signatures in humans. Science *328*, 235–239.

McLean, C.Y., Bristor, D., Hiller, M., Clarke, S.L., Schaar, B.T., Lowe, C.B., Wenger, A.M., and Bejerano, G. (2010). GREAT improves functional interpretation of cis-regulatory regions. Nat. Biotechnol. *28*, 495–501.

McVicker, G., van de Geijn, B., Degner, J.F., Cain, C.E., Banovich, N.E., Raj, A., Lewellen, N., Myrthil, M., Gilad, Y., and Pritchard, J.K. (2013). Identification of genetic variants that affect histone modifications in human cells. Science *342*, 747–749.

Meissner, A., Mikkelsen, T.S., Gu, H., Wernig, M., Hanna, J., Sivachenko, A., Zhang, X., Bernstein, B.E., Nusbaum, C., Jaffe, D.B., et al. (2008). Genome-scale DNA methylation maps of pluripotent and differentiated cells. Nature *454*, 766–770.

Nolte, J. (2009). The Human Brain: An Introduction to Its Functional Anatomy, Sixth Edition (Philadelphia: Mosby/Elsevier).

Odom, D.T., Dowell, R.D., Jacobsen, E.S., Gordon, W., Danford, T.W., Macisaac, K.D., Rolfe, P.A., Conboy, C.M., Gifford, D.K., and Fraenkel, E. (2007). Tissue-specific transcriptional regulation has diverged significantly between human and mouse. Nat. Genet. *39*, 730–732.

Ostuni, R., Piccolo, V., Barozzi, I., Polletti, S., Termanini, A., Bonifacio, S., Curina, A., Prosperini, E., Ghisletti, S., and Natoli, G. (2013). Latent enhancers activated by stimulation in differentiated cells. Cell *152*, 157–171.

Rada-Iglesias, A., Bajpai, R., Swigut, T., Brugmann, S.A., Flynn, R.A., and Wysocka, J. (2011). A unique chromatin signature uncovers early developmental enhancers in humans. Nature *470*, 279–283.

Rovsing, L., Clokie, S., Bustos, D.M., Rohde, K., Coon, S.L., Litman, T., Rath, M.F., Møller, M., and Klein, D.C. (2011). Crx broadly modulates the pineal transcriptome. J. Neurochem. *119*, 262–274.

Sanyal, A., Lajoie, B.R., Jain, G., and Dekker, J. (2012). The long-range interaction landscape of gene promoters. Nature *489*, 109–113.

Satake, W., Nakabayashi, Y., Mizuta, I., Hirota, Y., Ito, C., Kubo, M., Kawaguchi, T., Tsunoda, T., Watanabe, M., Takeda, A., et al. (2009). Genome-wide association study identifies common variants at four loci as genetic risk factors for Parkinson's disease. Nat. Genet. *41*, 1303–1307.

Schmidt, D., Wilson, M.D., Ballester, B., Schwalie, P.C., Brown, G.D., Marshall, A., Kutter, C., Watt, S., Martinez-Jimenez, C.P., Mackay, S., et al. (2010). Five-vertebrate ChIP-seq reveals the evolutionary dynamics of transcription factor binding. Science *328*, 1036–1040.

Shen, Y., Yue, F., McCleary, D.F., Ye, Z., Edsall, L., Kuan, S., Wagner, U., Dixon, J., Lee, L., Lobanenkov, V.V., and Ren, B. (2012). A map of the cis-regulatory sequences in the mouse genome. Nature *488*, 116–120.

Simón-Sánchez, J., Schulte, C., Bras, J.M., Sharma, M., Gibbs, J.R., Berg, D., Paisan-Ruiz, C., Lichtner, P., Scholz, S.W., Hernandez, D.G., et al. (2009). Genome-wide association study reveals genetic risk underlying Parkinson's disease. Nat. Genet. *41*, 1308–1312.

Stefanis, L. (2012). α-Synuclein in Parkinson's disease. Cold Spring Harb. Perspect. Med. *2*, a009399.

Sur, M., and Rubenstein, J.L. (2005). Patterning and plasticity of the cerebral cortex. Science *310*, 805–810.

Thomas, T., Timmer, M., Cesnulevicius, K., Hitti, E., Kotlyarov, A., and Gaestel, M. (2008). MAPKAP kinase 2-deficiency prevents neurons from cell death by reducing neuroinflammation—relevance in a mouse model of Parkinson's disease. J. Neurochem. *105*, 2039–2052.

van de Werken, H.J., de Vree, P.J., Splinter, E., Holwerda, S.J., Klous, P., de Wit, E., and de Laat, W. (2012). 4C technology: protocols and data analysis. Methods Enzymol. *513*, 89–112.

Visel, A., Minovitsky, S., Dubchak, I., and Pennacchio, L.A. (2007). VISTA Enhancer Browser—a database of tissue-specific human enhancers. Nucleic Acids Res. *35*, D88–D92.

Visel, A., Blow, M.J., Li, Z., Zhang, T., Akiyama, J.A., Holt, A., Plajzer-Frick, I., Shoukry, M., Wright, C., Chen, F., et al. (2009). ChIP-seq accurately predicts tissue-specific activity of enhancers. Nature *457*, 854–858.

Visel, A., Taher, L., Girgis, H., May, D., Golonzhka, O., Hoch, R.V., McKinsey, G.L., Pattabiraman, K., Silberberg, S.N., Blow, M.J., et al. (2013). A high-resolution enhancer atlas of the developing telencephalon. Cell *152*, 895–908.

Wang, Z., Zang, C., Rosenfeld, J.A., Schones, D.E., Barski, A., Cuddapah, S., Cui, K., Roh, T.Y., Peng, W., Zhang, M.Q., and Zhao, K. (2008). Combinatorial patterns of histone acetylations and methylations in the human genome. Nat. Genet. *40*, 897–903.

Ward, L.D., and Kellis, M. (2012). HaploReg: a resource for exploring chromatin states, conservation, and regulatory motif alterations within sets of genetically linked variants. Nucleic Acids Res. *40*, D930–D934.

Wu, T., and Hallett, M. (2013). The cerebellum in Parkinson's disease. Brain *136*, 696–709.

Zhu, J., Adli, M., Zou, J.Y., Verstappen, G., Coyne, M., Zhang, X., Durham, T., Miri, M., Deshpande, V., De Jager, P.L., et al. (2013). Genome-wide chromatin state transitions associated with developmental and environmental cues. Cell *152*, 642–654.